PCCP

PAPER

View Article Online
View Journal | View Issue

Cite this: *Phys. Chem. Chem. Phys.*, 2015, **17**, 27642

Light emitting diodes based on carbon dots derived from food, beverage, and combustion wastes

Prashant K. Sarswat* and Michael L. Free

Received 11th August 2015,
Accepted 21st September 2015

DOI: 10.1039/c5cp04782j

www.rsc.org/pccp

One important resource for material synthesis is waste. Utilization of waste as a resource for material synthesis is an environmentally responsible approach that reduces the need for virgin resources and subsequent processing. In this report a method to produce multicolored, luminescent carbon dots (CDs) and subsequent fabrication of light emitting diodes from food, beverage, and combustion wastes, is discussed. Apart from food and beverages, combustion exhaust was also utilized for CDs production. Optical characterization results suggest that CDs from waste food and beverages are more luminescent than those produced from combustion waste.

1 Introduction

Food and beverage waste is a matter of great concern. A 2014 United States Department of Agriculture (USDA) report suggests that ~31% of food produced was not available for human consumption at the retail and consumer levels.[1] Food and waste disposal in landfills is a significant source of methane[2] which has 21 times more global warming potential than CO_2.[2] Environmental, social and economic benefits are equally important when considering food waste mitigation. In the case of soft drinks, 2009 data suggests that carbonated soft drinks accounted for more than 70 billion USD.[3] Surprisingly, a large amount of carbonated liquid waste is generated by bottling plants, consumers, or retailers. Food and beverage waste can be anaerobically digested or recycled for uses such as fertilizer, animal feed or renewable energy generation, although such usage is low.[2]

In this paper, we demonstrate the use of food and beverage waste for the production of luminescent carbon dots (CDs) and subsequent fabrication of light emitting diodes (see Fig. 1). Apart from waste food and beverages, we have also utilized carbon fumes collected from burning samples of coal, wood, paper, and fuel. Utility of exhaust carbon fumes for CDs production also provides a new method of carbon capture.[4] CDs have been produced from various carbonaceous sources such as humic substances,[5] gelatine,[6] pericarp,[7] graphite powder,[8,9] and other source of citrus material.[10] These CDs can be synthesized using methods such as chemical ablation,[8] electrochemical carbonization,[8] laser ablation,[8] microwave[11] irradiation,[8] or solvothermal treatment. History of carbon dots starts from its first synthesis during carbon nanotube purification using an electrophoresis technique.[8] Later, other techniques such as laser ablation of graphite, were conducted to synthesize CDs. It is also a surprising that carbon is mostly found as a black powdery material or in its bulk counterpart (such as coal) and it exhibits weak luminescence, and low solubility in water. Contrarily, many of the CDs can be easily dissolved in a variety of solvents, depending on the nature of synthesis.[8] Fluorescence performance of CDs is also significantly higher than black carbon powder. Hence, remarkable

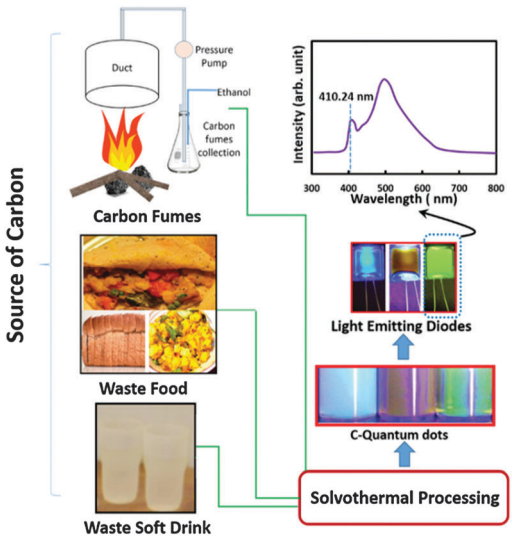

Fig. 1 A schematic diagram showing method and utility of waste food, drinks, and carbon fumes for light emitting diodes fabrication.

Department of Metallurgical Engineering, University of Utah, Salt Lake City, UT 84112, USA. E-mail: prashant.sarswat@utah.edu

research was done in last 10 years to improve the properties and the performance of CDs. Some of the advantages of CDs are their high aqueous loading capability, low toxicity, and good biocompatibility that enables them to be used in a variety of applications including sensing, catalysis, photovoltaics, and optoelectronics. In the case of the bottom up method of CDs synthesis, formation of CDs occurs through the rapid agglomeration of the carbonaceous material, derived from methods such as decomposition, pyrolysis, microwave treatment, or hydrothermal treatment of small organic molecules.[12] Broad optical absorption is one of the special features of the CDs that primarily originates due to π-plasmon and fluorescence linked to surface, edge, or structural defects.[13] The role of defect states and the origin of excitation wavelength dependence of CDs emission have been discussed in earlier literature.[14] Very limited research has been performed to examine the inhomogeneous distribution of CDs and the associated quantum confinement effect. Some of the CDs show the size dependent emission and excitation wavelength independent emission whereas some of the reports shows that CDs exhibit a red shift with increase in size as well as excitation wavelength.[14] Techniques such as single particle microscopy reveal that the excitation wavelength dependent emission of ensemble CDs is due to aggregate emission from the subset of CDs of different size. In this report also a few experiments have been conducted to evaluate the ensemble photoluminescence of CDs and origin of emission.

For enhancement of photoluminescence properties and stability, various strategies have been applied. Among them, N-doping, surface passivation, and functionalization using diamine-terminated oligomeric poly(ethylene glycol) ($\langle n \rangle \sim 35$, PEG_{1500N}) were proven to be successful.[9,12] In some cases the presence of carboxylic (–COOH) and hydroxyl (–OH) groups makes CDs highly luminescent due to surface defects induced by surface oxidation.[14] Many different strategies have been applied for N-doping that includes electrochemical methods, pyrolytic decomposition, and micro-emulsion polymerization.[12] In these cases optoelectronic and luminescent behaviour of doped CDs were found to be superior to undoped CDs. One of the explanations for better optical properties is the separation of electron–hole pairs due to differently charged surface groups.[15] It indicates that doped and surface functionalized CDs and associated techniques including new precursors, can still be explored, to observe any change in optical performance and luminescence behaviour.

In addition, CDs derived from the food and beverage waste without using toxic or human 'unsafe precursors', may be more safe, compared to that prepared from using corrosive solutions such as nitric acid.[16] It is important to note that immune activities of normal BALB/c mice could be affected due to the doses of CDs, though observed effects were not sufficient to alter the morphological change in their immune organs.[16]

Though many of the approaches are available to synthesize CDs, the easiest soft chemical preparation approach, solvothermal synthesis, is considered the simplest due to low cost apparatus, low energy consumption, good selectivity, and reduced number of preparation steps.[6] In this report also, we have utilized the solvothermal approach for CDs synthesis.

2 Experiments

Waste food was washed thoroughly to remove any dust and other impurities prior to CDs synthesis. Tortilla and bread pieces (total weight ~5 gm) were sorted from waste and small pieces (3–8 mm) were made, so that these pieces can be easily inserted in the reaction vessel. In a typical experiment, 2 ml of 1-dodecanol, 30 ml of absolute ethanol and 0.05 ml of oleic acid were mixed and used as a precursor solvent. This mixture was heated in an argon atmosphere for 1.5 hours at a temperature of 200 °C. At this temperature ethanol starts evaporating; hence additional ethanol was inserted into the reaction vessel. It was observed that more than ~90% of the tortilla pieces were either untreated or partially reacted. This residue can be further utilized as a source of energy that has a heat of combustion value of ~4500 Cal gm^{-1}.[17] Direct heating of 20 ml of carbonated soft drink (temperature ~170 °C) for ~30 minutes also results in the formation of C-dots (but these have relatively lower emission performance). Similarly, C-dots can also be synthesized using microwave oven. 20 ml of soft drink was heated in microwave safe beaker. The technical details of the microwave oven made by sharp is 120 V, 60 Hz/1.67 kW, 14.5 A.

In the case of soft drink utilization, 15 ml of soft drink was mixed with 20 ml of ethanol and 0.05 ml of oleic acid. This mixture was heated for 1.5 hours at a temperature of ~230 °C. It was observed that the viscosity of the reaction mixture started increasing after ~1 hour of heating. After 1 h of heating nucleation and growth need to be carefully controlled by lowering the temperature. Initially, the reaction mixture was transparent then it turned into a light yellow transparent semisolid, indicating completion of the reaction. Continuous irradiation of UV light in the reaction chamber provided a good way to monitor CDs formation. Initially, the reaction chamber showed light blue emission that changed to green and subsequently yellow-green very rapidly. The synthesis reaction was quenched when the desired color was obtained and the samples were diluted with absolute ethanol. It was interesting to observe that a viscous CDs mixture can be mixed with water to reduce its viscosity. In the case of combustion product waste, exhaust gases from burning samples were slowly mixed with ethanol.

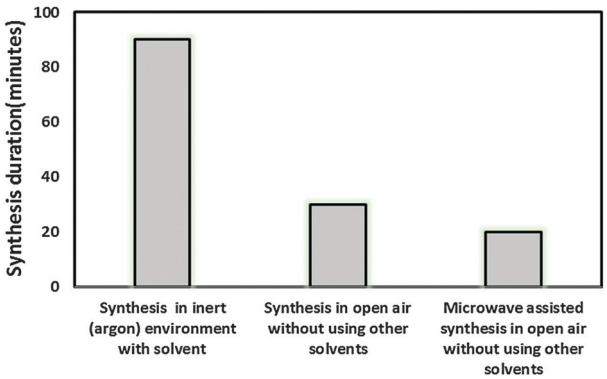

Fig. 2 A comparison of synthesis duration of C-dots from different methods.

The resulting mixture was blended with 0.05 ml of oleic acid and gently heated in an inert environment for 45–60 minutes. This sample also showed green-yellow luminance during UV irradiation. Red color quantum dots were produced using, 5 ml of phosphoric acid that was mixed with 2 ml of ethylene glycol, 15 ml of waste soft drink, and 0.05 ml of oleic acid. The other reaction parameters were kept similar to the other described synthesis methods. Synthesis time was reduced significantly when a microwave assisted synthesis method was adopted (see Fig. 2).

3 Instruments and characterization

Fourier transform infrared (FTIR) spectra were recorded for waste soft drink in the wavenumber range of ~4000–600 cm^{-1} using a PerkinElmer Frontier™ FTIR spectrophotometer equipped with an ATR accessory and Spectrum 10™ software suite. X-ray photoelectron spectroscopy (XPS) survey spectrum was recorded using the monochromatic Al-Kα source equipped Kratos Axis Ultra DLD instrument. Raman spectra were acquired using an R 3000 QE Raman spectrometer in backscattering mode. The excitation wavelength was ~785 nm and the laser power was ~100 mW, for Raman measurements. Optical characterizations were conducted using an Ocean Optics spectrophotometer and an Avantes spectrophotometer in the range 300–800 nm using quartz cuvettes. For emission spectra, a range of excitation wavelength (360–650 nm) was utilized. Atomic force microscopy was conducted using a JPK Instruments NanoWizard 3a ultra AFM. Transmission electron microscopy was carried out using an FEI 200 keV Tecnai G2 F20 transmission electron microscope. Additional experiments for CDs size analysis were performed using a Shimadzu-SALD particle size analyzer equipped with WingSALD II software.

4 Results and discussion

Understanding of the properties of the CDs, derived from the sources that contain a variety of the constituents and precursors, is more challenging compared to that derived from a known source of a well-defined chemical composition. In this section most of the common optical properties are examined and a comparison was done with many of the well-studied CDs optical properties. It is important to mention that some of the properties of CDs derived from a waste cannot be a 'sole' characteristics of CDs, as there might be some presence of impurities or other trace material. In upcoming sections, more focus was given for CDs, synthesized from soft drink using a routine solvothermal process.

4.1 FTIR and XPS spectroscopy examination

Soft drink contains a variety of components including sugar, gasified filtered water, acidifier, and conservator.[18] An FTIR spectrum (Fig. 3) shows intense peaks at ~1029 cm^{-1}, 1096 cm^{-1}, 1206 cm^{-1}, 1325 cm^{-1}, 1452 cm^{-1} and 1652 cm^{-1}. These peaks indicate the presence of citric acid (1325 cm^{-1}), caffeine (1029 cm^{-1} minor stretching of C–C bond), 1652 cm^{-1}

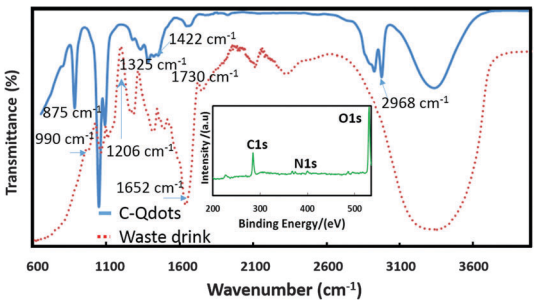

Fig. 3 FTIR spectroscopy results of waste soft drink samples. XPS measurements results are shown in inset of figure.

(possibly due to the stretching vibration of carbonyl groups of caffeine), and sugar (shoulder at 1052 cm^{-1}: C–O stretch; D-fructose shoulder at 990 cm^{-1}: CH_2 out of plane deformation; and shoulder at 1131 cm^{-1}: C–O–C antisymmetric stretch).[19–21] Peaks at 1700–1750 cm^{-1}, indicate the presence of ester groups.[22] This FTIR and literature examination suggest that waste soft drinks contain a variety of carbonaceous source including trace level organic compounds,[23] however, we believe that sucrose and D-fructose dissolved in soft drinks, are the main source for CDs production. XPS analysis (see inset of Fig. 3) of CDs shows dominant peaks at 531.5 eV, 399.1 eV, and 284.8 eV, that can be attributed to O1s, N1S, and C1s. An FTIR spectrum of CDs sample indicates peaks at 1090 cm^{-1} and 875 cm^{-1} (oxygen containing groups); 1422 cm^{-1} and 2968 cm^{-1} (alkyl and aryl groups) and a broad peak ~3050–3600 cm^{-1} (possibility of amine containing groups). All of this information indicates the formation of CDs.[6]

4.2 AFM and TEM examination

For AFM imaging, an atomically flat mica substrate was acquired and CDs were immobilized on the substrate using the diluted synthesis solution. A BudgetSensor Multi75E-G sample (f = 75 kHz, k = 3 N m^{-1}, Pt/Cr coating) type cantilever was utilized. Fig. 4a and b shows height information and 3D rendering for a 1 μm × 1 μm sampling area. AFM height information, 3d rendering, and TEM images (Fig. 4c) indicate that the size of these CDs ranged from 4 nm to 20 nm. Fig. 4d shows high resolution TEM image of green carbon CDs showing a lattice parameter of 0.24 nm, which matches well with the reported parameter for luminescent carbon dots.[24]

4.3 Optical properties

Fig. 5a shows normalized absorbance spectra of CDs in ethanol solution. It can be seen that all CDs show strong absorbance in the UV range, and their tail extends into the visible range. Integrated absorbance was highest for red CDs obtained using soft drink and phosphoric acid. The lowest absorbance was recorded for CDs obtained using waste food (CDWF). From emission spectra (Fig. 5b) it was observed that the intensity of CDWF was relatively higher than that of CDs obtained from waste soft drink (CDSD). Emission intensity was lowest for red CDs. Photostability measurements were also performed for CDs

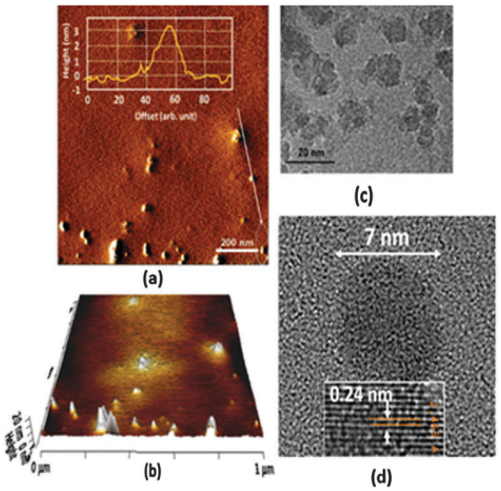

Fig. 4 (a) Height information from atomic force micrograph of CDs immobilized on mica substrate, (b) corresponding 3D rendering, (c) TEM image of CDs, and (d) high resolution TEM image of 7 nm size C-dot.

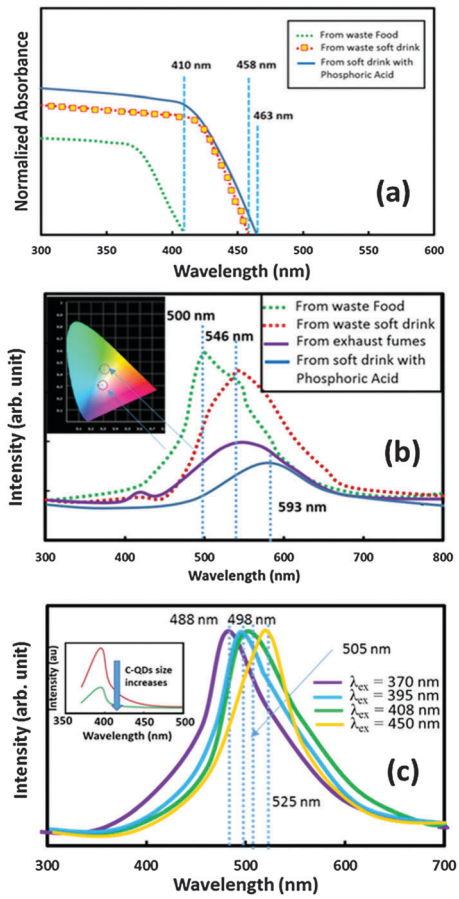

Fig. 5 (a) Absorbance and (b) emission spectroscopy results for different type of C-dots solutions. (c) Normalized emission spectra for different excitation wavelength irradiation for CDSD. Inset of Fig. 4c shows the variation in emission peak intensity with respect to excitation wavelength.

in ethanol solution under continuous illumination of visible light for 12 hours. It was observed that CDWF and CDSD were more photostable compared to red CDs. The reduction in emission peak intensity was ~10% and 30% for CDWF and red CDs, respectively. Such low emission intensity and reduced photostability for red CDs can be attributed to fluorescence quenching, due to excess of phosphoric acid as evidenced in Raman characterization.[25,26] Further analyses of emission spectra suggested that full width at half maximum (FWHM) of emission peak for CDWF was not significantly different than that peak obtained from CDSD. In contrast emission peaks were smaller for CDs obtained from combustion exhaust (CDEF) as well as red QDs. CDWF emission peak was centered at ~500 nm, CDEF and CDSD peaks were centered at ~546 nm, and for red CDs the peak was centered at ~593 nm. In Fig. 5b inset, a chromaticity diagram is shown. Red shifting of the emission peak indicates an increase in size of CDs. Fig. 5c shows normalized emission spectra recorded for CDSD, which will be further investigated in the next section. The fluorescence of CDSD solution during the CDs growth indicates that emission intensity was highest for the initial set of data and it reduces subsequently as growth proceeds (see Fig. 6). An emission peak was observed at ~515 nm for a sample that was collected first and within ~5–6 minute, the emission peak shifted towards the higher wavelength. For bigger size dots (or CP) emission peak intensity was lower and such a peak was located at ~610–625 nm. FWHM for the initial sample (emission peak ~515 nm) was ~100 nm, which matches well with earlier reports for carbon dots and indicate a broad size distribution.[9]

4.4 Raman examination

A systematic Raman examination (Fig. 7) of soft drink (without adding solvent) as well as reaction products (after its evaporation), were also conducted. Initially, peaks were observed at ~298 cm^{-1}, 373 cm^{-1}, 1261 cm^{-1}, 1330 cm^{-1}, that were later disappeared as mixture evaporates. Disappearance of peaks at ~372 cm^{-1} and 1261 cm^{-1} indicates the decomposition or evaporation of sorbic acid.[27] Some additional peaks at ~1124 cm^{-1} (glucose) and 750 cm^{-1} (citric acid) were observed for sample collected after a few minutes of heating.[28] Distinct peaks were observed at

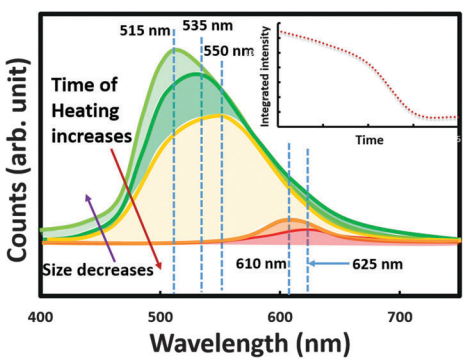

Fig. 6 Emission spectra of C-dots of different size (these spectra were acquired by rapid collection of C-dot solution from reaction mixture during growth). A red shift was observed for emission peak during growth. Inset of figure shows a variation in integrated intensity of CDs, as growth proceeds.

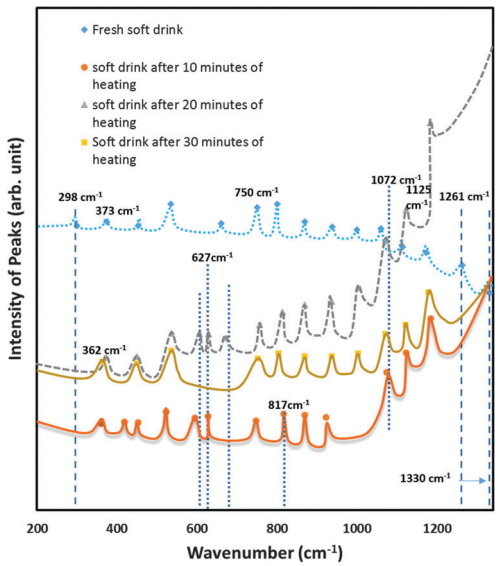

Fig. 7 Peak intensity–wavenumber graphs derived from Raman spectrum for individual samples (fresh soft drink and evaporated soft drink solution). It can be seen that few peaks completely disappear and some new peaks appear after evaporation.

$\sim$627 cm^{-1} (fructose), 817 cm^{-1} (fructose), 868 cm^{-1} (fructose), 1072 cm^{-1} (fructose), 1125 cm^{-1} (glucose) for evaporated viscous mixtures.[28] An excess of these residual compounds and coarse nanocrystals clusters causes the reduction in effective quantum efficiency of CDs.[10] Raman examination of the red CDs mixture (Fig. 8) shows the peaks at $\sim$890.76 cm^{-1}, 1005 cm^{-1}, and 1176 cm^{-1}. These peaks correspond to $\nu_s P(OH)_3$, $\nu_{as} P(OH)_3$, and $\nu P{=}O$, respectively. These different modes are due to the P–O stretching region of H_3PO_4.[29] Few low intensity peaks or shoulders were observed at $\sim$877 cm^{-1} and 940 cm^{-1} to indicates the presence of $H_2PO_4^-$ (aq) in the CDs mixture[7].

4.5 Investigation of mechanism of formation and emission

The mechanism of CDs formation, in cases of pyrolysis of citric acid, has been explained.[8] It is believed that at temperatures greater than 200 °C, growth of a carbonaceous core starts. The observed emission at this stage is jointly due to emission from the molecule fluorophores and from the carbonaceous core. In the case of higher temperature synthesis, the origin of the emission is mainly from the carbonaceous core. For smaller size CDs, the surface layer contains more atoms that provide more contribution from the surface, compared to the interior due to their finite size. As can be seen in our case, Raman and FTIR examination clearly suggest the pyrolysis of few organic acids and intensification of some peaks that supports the theory of a carbonaceous core. For better understanding, excitation wavelength and power dependent emission measurements were performed. For the first set of experiments, seven different wavelength excitation (λ = 370 nm, 395 nm, 408 nm, 450 nm, 500 nm, 545 nm, and 652 nm) sources (see their respective normalized spectra, Fig. 9) were used for emission measurements. Fig. 5c shows corresponding normalized emission spectra. It was observed that the emission intensity (see inset of Fig. 5c) first increases and subsequently decreases; emission intensity for 545 and 652 nm wavelength excitation was very insignificant. Such a trend was consistent for small as well as relative big size CDs. The emission peak position for each set of measurements was also monitored. It was observed that emission maxima strongly depends on the excitation wavelength and such a dependence was more prominent in the case of small size CDs (see Fig. 10). One emission peak exhibited a shift from 488 nm to 530 nm, when the excitation wavelength was varied from 370 nm to 545 nm. For CDs obtained from the combustion waste, such a shift was more confined and varies from $\sim$520 nm to 550 nm when the excitation wavelength was varied from 370 nm to 545 nm. In the present case, the excitation is above 300 nm, and hence, excitation of the CDs carbogenic core is neglected.[14] In such a case, (excitation is much greater than 320 nm) it can cause excitation followed by emission from surface trap states. Information from Fig. 10 suggests that for bigger size CDs, the rate of change of emission wavelength was not as high as that for small size CDs. A careful examination of Fig. 10 suggests that

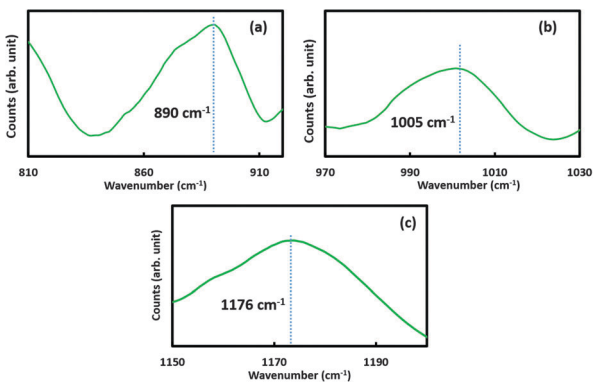

Fig. 8 Raman spectroscopy results for red color C-dot sample. The peaks or shoulder at $\sim$877 cm^{-1}, 890.76 cm^{-1}, 1005 cm^{-1}, and 1176 cm^{-1} indicate the presence of H_3PO_4 or $H_2PO_4^-$.

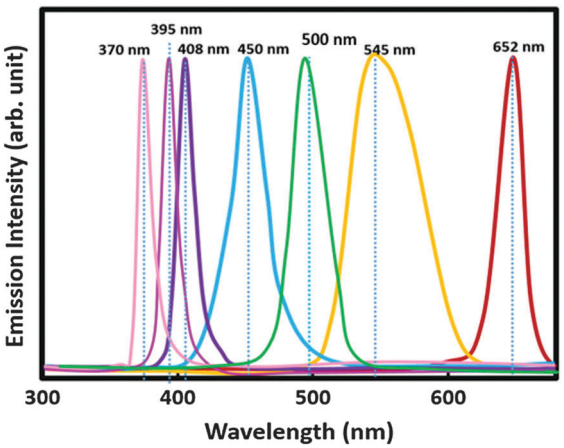

Fig. 9 A figure showing normalized spectra for different excitation source, collected at scope mode.

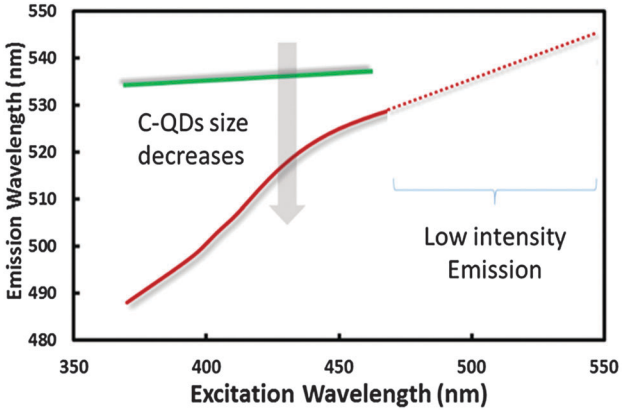

Fig. 10 Emission peak wavelength *vs.* excitation wavelength relationship for C-dot solutions. It was observed that emission peak intensity was very less when excitation wavelength exceeds 450 nm, hence these data are shown as discontinuous line.

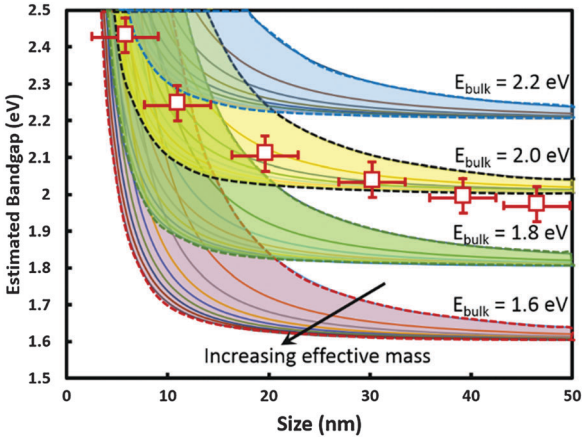

Fig. 11 Energy bandgap–C-dot size relationship graphs, simulated for different sets of bulk band gap and effective mass. Each shaded region corresponds to a particular bulk-bandgap value. White squares represent the actual experimental data points.

the gradient of emission wavelength change is inversely related to the size of CDs.

A shift of an emission peak generally indicates the presence of the multi-fluorescence centers and a possibility of attachment or the removal of the functional groups. Such an assumption was well validated in density functional theory calculation results.[30] However, for the bigger size CDs, the rate of change of emission wavelength and the red shift of more than ~50 nm indicates the reduction in mean lifetime (τ_m) of photoluminescence.[30] Shorter τ_m generally indicates a direct electron–hole recombination, while longer τ_m can be viewed as the slow process of energy loss due to electron–hole pair localization at defect states and subsequent emission of photons.[30] As can be seen from Fig. 5, 6 and 10, relatively large CDs emit longer wavelength photons that generally have shorter τ_m.[30] This suggests a core related emission. However, this assumption will not be valid in cases when τ_m is longer.

The broad emission spectra indeed indicated the distribution of different emissive sites on the C-dots. One of the concerns is, excitation wavelength–emission wavelength/intensity dependence is due to quantum effect or due to emissive traps on C-dot surface, defect energy trapping (DET) states, or any other unexplored mechanism, is still a matter of debate. However, the majority of reports accept a 'defect-derived photoluminescence' mechanism for CDs. This acceptance can be further strengthened by considering the fact that defect derived luminescence is much brighter compared to that of bandgap-based fluorescence.[31] Ultrafast spectroscopy based data and analysis also suggested that edge states, emission centers, and traps are the dominating reasons for the green luminescence and optical properties of C-dots.[32] Hence, additional analysis and theoretical calculations have been performed for better understanding of emission and the emission-CDs size relationship. HOMO (highest occupied molecular orbital)–LUMO (lowest unoccupied molecular orbital) gap of CDs was calculated and a relationship between size and the gap is plotted. It can be seen that the gap increases gradually with a decrease in size of CDs. It clearly indicates a strong contribution in emission originates from the quantum size of carbon dots.[33] The Brus equation can be utilized to evaluate particle size-band gap relationship:[34]

$$E_g(\text{CDs}) = E_g(\text{bulk}) + \left(\frac{h^2}{8R^2}\right)\left(\frac{m_h + m_e}{m_h m_e}\right) - \frac{1.8e^2}{4\pi\varepsilon_o\varepsilon_R R} \quad (1)$$

where m_h and m_e are effective hole and electron mass respectively, R is the radius of C-dots, h is the Plank constant, e is the charge of electron, E_g is the energy bandgap, ε_r denotes relative permittivity, and ε_0 is free space permittivity.

Eqn (1) was derived using model Hamiltonian and it also considers the shielded Coulomb interaction.[34] This equation clearly indicates that with the increase in particle size, the contribution from the second term decreases, whereas the third term effective contribution increases the band gap due to its negative sign. As can be seen (Fig. 6 and 11), band gap increases with decrease in CDs size, hence only first two terms were considered in the analysis. In most of the cases examined for several materials, eqn (1) shows an asymptotic approach towards the bulk band gap when size increases. A modified version of eqn (1) can be written as:

$$E_g(\text{CDs}) = E_g(\text{bulk}) + \Delta E_{\text{Confinement}} \quad (2)$$

In case of a cube-box type problem $\Delta E_{\text{Confinement}}$ can be written as:[35]

$$\Delta E_{\text{Confinement}} = \frac{3\hbar^2\pi}{2m^* d^2} \quad (3)$$

where d is the size of particle, $\hbar$ is the reduced Plank's constant, and m^* is the reduced effective mass of the system. In order to provide a graphical representation of eqn (3), effective mass of electron and hole are needed. We have used a range of effective mass, discussed in the literature[36] for simulation. The results of simulation suggest that in most cases, effective mass varies between 0.03 m to 0.1 m.[36,37] In case of zigzag carbon nanotubes, there was not much difference in the effective mass of hole and electrons except in (7, 0) and (8, 0) chirality.[38] Hence,

for our analysis, we assumed $\sim m_h \sim m_e$. Another challenge for this simulation is obtaining information about the bulk band gap value. Various types of amorphous carbon and graphite exhibit zero band gap. Quantum effects appear when size of carbon particles reduces, reports suggest.[39,40] In some cases a high band gap ~8.5 eV was predicted for carbon cluster containing less than 10 atoms, whereas in most cases it is suggested that the HOMO–LUMO gap value between ~1.6 eV to 2.2 eV for the carbon clusters containing more than 60 atoms.[41,42] Hence, we can consider the estimated bulk energy bandgap in these ranges and can plot the size-bandgap relationship. We have chosen four sets of bulk bandgap values ~1.6 eV, 1.8 eV, 2.0 eV, and 2.2 eV (see Fig. 10). For simulation, nine different values of the effective mass were chosen with the lowest equal to ~0.01 m, and the highest equal to ~0.09 m. Fig. 11 shows the four different regions, (corresponds to four different bulk bandgap) and their bandgap-size relationship. It is interesting to observe that for size less than 10 nm, there is very good overlap in these regions. In this situation, it will be difficult to find the best fitting parameters for experimental data. Hence we have chosen an extended range and imposed actual data points (see squares) on it. From a least squares fitting analysis, it can be concluded that estimated bulk bandgap value for C-dots is ~1.9 eV, whereas the value of effective mass is ~0.03–0.04 m.

For further assessment of the emission behaviour of soft-drink derived CDs, we have monitored emission wavelength intensity for the normalized excitation signal. These examinations were done for different sizes of CDs (see Fig. 12). It can be seen that the peak intensity increases up to a certain value of wavelength and subsequently decreases. It is interesting to observe that such a trend was very strong for relatively small size CDs.

For big size CDs the rate of intensity variation was much lower than their small counterparts. Such an excitation dependent emission behavior can be viewed as a 'multiple transition mode' exhibited by the CDs.[43] In the case of multiple transition mode, the emission peak also shifts towards longer wavelengths with an increase in excitation wavelength, as already presented in Fig. 5c and 10. It is important to mention the difference between the behaviors of small size CDs and bigger CDs. Though the peak intensity exhibits a maxima for a certain wavelength ~(390–400 nm) for big size CD, emission peak wavelength shows the almost excitation independent behavior. It can be viewed as 'single transition mode' for big size CDs emission.[43] As mentioned in our earlier discussion that surface state density/volume of CDs is much enhanced in the case of small size CDs. One of the major roles of these surface states or defect states is to create the emission levels between HOMO–LUMO gaps. The occurrence of transition between these states possesses a different probability for different excitation wavelength. Hence excitation dependent emission also shows a variation in peak intensity. In case of small size CDs surface state based transition and energy gap transition are major contributors for emission whereas for big size CDs single state transition dominates. In case when energy of excitation is more than the bandgap of CDs, emission originated from energy-band gap transition dominates. In contrast, surface states based transition contributes significantly for the opposite case (when excitation energy is less than bandgap). Such a process can be well validated by observing the two regions in Fig. 12. It can be seen that for big size CDs the rate of intensity variation moreover remains constant after the excitation wavelength exceeds a certain value. This further validates the assumption of a lower contribution from the surface states for big size CDs. We can express our explanation in equation form:

$$\text{Intensity(CDs)} = F(\text{bandgap}) + G(\text{surface states}) \quad (4)$$

The maxima of the intensity variation curve can be calculated by differentiating the equation with respect to wavelength:

$$\frac{d\text{Intensity(CDs)}}{d\lambda} = \frac{dF(\text{bandgap})}{d\lambda} + \frac{dG(\text{surface states})}{d\lambda} \quad (5)$$

It can be further written as:

$$\frac{d\text{Intensity(CDs)}}{d\lambda} = \frac{dF(\text{bandgap})}{d\lambda} + \frac{dH(\text{probability})}{d\lambda} \quad (6)$$

where 'F' and 'G' represent the function of the bandgap and surface states, respectively. As, surface states are further linked with their transition probability, we used another symbol 'H' for this dependence. It can be seen that there is a very small shift in peak position with size variation of CDs, which clearly indicates that such a maxima least represent a band gap based contribution. Due to size variation, there is a variation of band gap also and such a variation should show a shift in peak position. However, the second term in eqn (6) represents a surface state contribution that is also related to transition probability for a particular excitation wavelength, which is moreover constant for different size CDs. Hence, it can be said that the transition probability for excitation wavelength (~390–400 nm) is highest for all sized CDs studied in this research.

Based on discussion in this section and preceding sections, and information from literature, a band diagram can be plotted that explains the overall emission process. A variation in

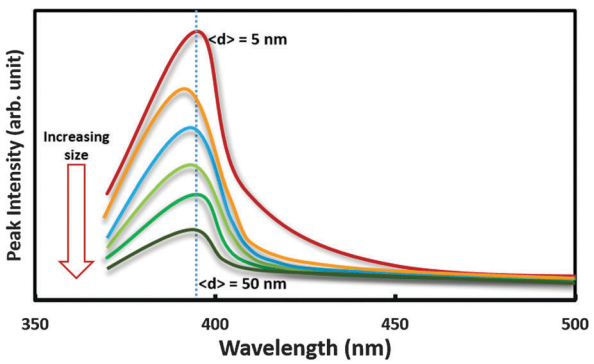

Fig. 12 Excitation wavelength–emission peak intensity behavior for different sized soft drink derived CDs. It can be seen that emission peak intensity exhibit a maxima for a certain wavelength excitation.

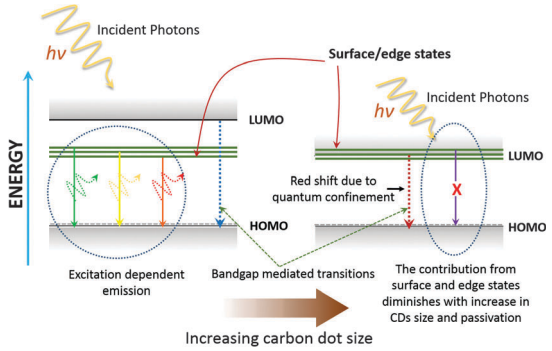

Fig. 13 Energy-band diagram for carbon dots of different size. It can be seen that excitation dependent emission is more prominent in small carbon dot due to a relative position of surface states with respect to LUMO as well as less passivation.

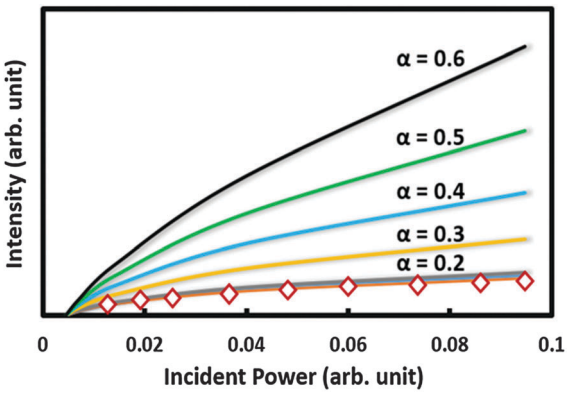

Fig. 14 Simulated data (continuous lines) for eqn (7) and normalized emission peak intensity–incident power relationship for C-dots, for 408 nm excitation (red diamond). A good fit can be seen for $\alpha \sim 0.2$.

emission characteristics and associated photophysics indicates the intrinsic and edge state dependencies with CDs diameter. With increase in CDs size and number of carbon atoms in dots, there is a possibility of reduction of intrinsic states.[44,45] A case when these intrinsic states relative position in the band diagram became lower than the edge state, there is a loss of expected emission.[44] One of the important parameters is the offset between energy levels (surface states and band position) that decide optical properties. An addition to this mechanism is the surface oxidation of CDs that is also responsible for band gap narrowing of the surface states.[46] Fig. 13 shows a band-diagram that shows fluorescence phenomenon for small and large CDs. It can be seen that for a small CDs, an offset between surface states and LUMO is higher compared to that of the relative large CDs. In this case emission wavelength is excitation wavelength dependent. However, with increase in size of dots, such a dependency weakens and the contribution of the first term in eqn (6) (band gap mediated transition) starts increasing. The hampering of surface state based transition as well as the presence of some functional groups causes 'excitation independent emission behavior'. It can be seen in the case of CDs with amino rich surface groups they exhibit less dependency on excitation wavelength due to passivation of surface states.[43] In case of soft drink/food waste derived CDs, there are many possibilities of such groups (discussed in Section 4.1 and 4.5) that can cause surface passivation. However, at present it will be premature to accurately conclude about the effects of functional groups.

Incident power variation (wavelength $\sim$400 nm) experiments were conducted and measurements were done to monitor the emission intensity. It can be seen (see Fig. 14) that the emission intensity increases rapidly, initially, and attains a saturation at certain stage. It clearly shows that CDs emission exhibit nonlinearity. Excitation density 'P' and integrated photoluminescence 'I' can be related as:[47]

$$I = P^{\alpha} \tag{7}$$

where exponent 'α' depends on the dominant charge carrier recombination process.

In many cases the emission intensity depends both on non-radiative rate and bimolecular radiative rate.[47] In these cases modified equations have been utilized. In the present case, non-radiative recombination limits the quantum efficiency (α is less than 1 in our case) when illuminated with high power excitation. This information also indicates a situation of 'quasi-equilibrium occupancy' of the local level by the non-equilibrium carriers.

Hence, based on the current set of data and our analysis, we believe that bandgap transitions or quantum size effects, or defect derived emission are not a single dominating mechanisms, governing the luminescence behavior of our C-dots. It is rather believed that two or more processes are responsible for emission from C-dots. Most of these observations and results match well with the findings of other researchers for the CDs optical properties.[9,48]

4.6 Measurement of quantum yield

For measurement of the quantum yield, a standard procedure was adopted. For a reference standard, quinine sulfate in 0.1 M H_2SO_4 was used (λ_{ex} = 360 nm). Efforts were given to avoid perturbation of quantum yield, by using standard 10 mm path length fluorescence cuvettes. Following formula was used for QY measurements:[49]

$$Q_{\text{measured}} = Q_{\text{ref}} \frac{I \varepsilon_{\text{ref}} n^2}{I_{\text{ref}} \varepsilon {n_{\text{ref}}}^2} \tag{8}$$

Here 'Q' represents the quantum yield, 'I' represents an integrated fluorescence intensity, ε represents extinction coefficient, and 'n' represents the refractive index. The index ref indicate the reference standard. Quantum yield was highest for waste food derived CDs $\sim$0.26. Food products derived from wheat grains contain several compounds of wide range of molecular weight, including polysaccharides, lipids, proteins, calcium, dispersed gelatinized starch granules, and fibrous material.[50] FTIR analysis suggests the presence of nitrogen from protein and amidic groups in wheat or wheat based products.[50] The presence of nitrogen containing groups enhances the possibility of N-doped CDs formation, as evidenced in earlier reports.[51,52] These doped

CDs are expected to exhibit better catalytic activity, transport properties, and enhanced luminescence.[53,54] Although wheat based foods contain a variety of carbonaceous compounds, it will be premature to decide the leading source for CDs formation and reaction mechanism. However, it is believed that elevated temperature and rigorous hydrothermal condition are the main source of energy that converts the mixture containing carbonaceous components into small carbon nuclei due to a nucleation burst.[55] Such a burst occurs when reaction mixture attains an adequate level of supersaturation.[55]

4.7 Fabrication of LED using C-dot based resin

LEDs have been fabricated using CDs and Zn doped $AgInS_2$ nanocrystals, and using a primary source of UV light.[56] It was reported that fabricated LEDs exhibited color rendering index (CRI) of ~96.[56] Such a CRI value is adequate for solid state lighting for true color representation. Another report discussed the fabrication of color switchable LEDs that were fabricated using CDs, conducting polymer hole injection layer, electron transport layer, anode, and cathode layers.[57] The maximum reported brightness for the white LEDs was ~90 cd m^{-2}. One of the challenge that encounters during fabrication of the LEDs is the reduction of luminescence after drying of CDs. Such a reduction is mainly due to aggregation induced quenching.[58] In case of static quenching, the mechanism can be explained on the basis of interruption to electron–hole radiative recombination.[59] The reduction of luminescence of carbon dots in the solid state often restrict their usage in fabrication and development of white LEDs. It was reported that fluorescence carbon dots can be directly utilized as a phosphor for the fabrication of LED without using a polymer to form composite. Here we have included some details about LED fabrication and their optical properties. Multi-color LEDs were fabricated using luminescent CDs, by preparing transparent sols or solid hosts. Such solid hosts can be prepared using an adequate mixture of Buhler epoxy resin and hardener. Primary CDs suspension was cleaned using multistep washing by dichloromethane and centrifuging. A Quantum dots suspension was mixed in $CHCl_3$ and subsequently mixed with Buehler Epothin epoxy resin. Such a mixture was slowly heated at a temperature of ~50 °C to remove volatile components. After slow heating for ~30 minutes, two different layers were observed. Each layer of resin-CDs mixture can be distinguished from the other by irradiating the solution with UV light. A useful layer was removed and epothin hardener was mixed with it (ratio ~ 5 : 2). This luminescent mixture and UV light LED can be utilized to fabricate different color LEDs using a small transparent enclosure and a lid (see Fig. 1). UV light LED (specification: wavelength = 400–410 nm, luminous intensity: 12 mW typ. @ 20 mA, peak forward current ~30 mA, power dissipation: 120 mW, forward drop ~3–3.5 V) was utilized as the primary source of illumination. After inserting UV-LED and luminescent mixture in enclosure, 24 hours curing was allowed to make hard and robust LEDs. The emission spectra for the different LEDs were recorded and for green LED it is shown in Fig. 1. It can be seen that emission peak extends from 350 nm to 650 nm, with highest intensity at ~510 nm, and FWHM of ~165 nm. A low intensity peak at ~410 nm was also observed, that corresponds to peak emission wavelength of UV-LED. Thickness dependent emission spectra (see Fig. 15) were recorded using LEDs prepared from CDs based highly viscous solid host. It was observed that with decrease in CDs host layer thickness, a slight blue shift occurs. The value of this blue shift ($\Delta\lambda$) was ~8–12 nm. We also observed a reduction in emission peak height when layer thickness decreases. Though mechanism of this shift was not fully explored in this paper, report[60] suggests that during the progressive propagation of emission to longer distance, there is an re-absorbance and re-emission of light in many times. After each cycle of emission, photon energy reduces. Such a reduction in photon energy is equal to the amount of stokes shift for the involved transition.[60] After several cycle of light emission and re-absorbance, that also include the populating of next highest level, through the photons from the previous cycle. This sequential process results in succession of the highest level.

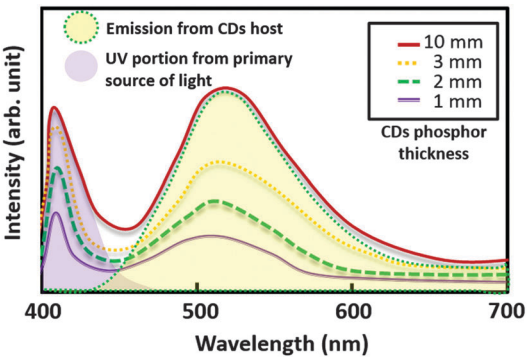

Fig. 15 Emission output as a function of wavelength for CDs based LEDs for different thickness of phosphor layer.

We have also investigated the colour gamut and chromaticity diagrams recorded using Oceanview 1.5.0 software (colour application wizard). It was observed that tint of most of the CDs based LEDs was greater than 120, (highest was 161) for LED fabricated using soft drink derived CDs. LEDs derived from the red CDs (phosphoric acid route) have a negative tint value. LED derived from food-waste CDs has a tint value of ~127. Excitation purity was highest (~0.51) for soft drink derived LED, whereas it was lowest (~0.30) for LED derived from phosphoric acid based red CDs. The whiteness value was highest (~382) for CDs derived from waste food. CDs derived from soft drink have a whiteness value of ~316. Solid state LED prepared using soft drink derived CDs shows a whiteness value of ~880. In most of the cases, for soft drink derived LEDs, we observed Commission Internationale de l'Eclairage (CIE) coordinate: (0.37, 0.53, 0.10). A huge variation in CIE coordinate can be obtained by changing the duration of CDs synthesis duration and route. CIE coordinate changes to (0.53, 0.42, 0.04), when red CDs based LEDs were examined. For yellow colour CDs based LED, obtained using soft drink, the CIE coordinate was ~(0.42, 0.48, 0.08). Earlier CIE chromaticity coordinate was reported ~(0.327, 0.324) that was close to ideal white colour,

however, these data were obtained using hybrid carbon dots.[54] In our case, both tint and whiteness values indicate that these LEDs can be categorized as blue-white light emitting LED. The positive value of tint in most of the cases indicates that red colour portion in their emitted light is minimum.

5. Conclusions

In summary, utilization of waste food, carbonated soft drinks, and combustion products for the synthesis of highly luminescent, multi-coloured carbon dots based light emitting diodes has been demonstrated. The emission spectra of these quantum dots suggest that the emission intensity for CDWF was highest, whereas red colour CDs showed less luminescence. Relatively lower photo-stability and emission intensity for red CDs can be attributed to fluorescence quenching caused by an excess of phosphoric acid or their ions. Most of our CDs exhibit excitation wavelength and size dependent emission behaviour. For relatively big size CDs, the emission wavelength shift was not very high compare to the small size counter parts when illuminated with different wavelength excitations. The Brus equation was utilized to explain quantum confinement behaviour and to estimate band gap and effective mass of CDs. Emission peak intensity was also monitored, and it shows a maxima at wavelength ~390–400 nm, for different sized CDs. It was concluded that the emission behaviour of these CDs cannot be explained by one mechanism. Incident power dependent emission measurements were also performed. These measurements indicate that non-radiative recombination limits the quantum efficiency of CDs. Our analysis suggests that two or more processes (such as surface states, quantum confinement, and bandgap based transition) are responsible for emission characteristics. The emission spectrum of a small light source, fabricated using UV-LED as a primary source, shows a broad peak centred at ~510 nm. Thickness dependent emission and colour analysis was also performed to further examine the quality of light emitted by the LEDs. Most of the LEDs can be categorized as 'bluish white' light type LEDs, based on tint and CIE whiteness data.

Acknowledgements

This work was partially supported from Techanaya LLC., Murray, UT. Nanoparticle characterizations were done at University of Utah. Atomic force microscopy was performed by a staff member of JPK Instruments (USA). TEM imaging was performed by Gaosong Yi (PhD Scholar, University of Utah).

References

1 J. C. Buzby, H. F. Wells and J. Hyman, *The Estimated Amount, Value, and Calories of Postharvest Food Losses at the Retail and Consumer Levels in the United States*, EIB-121, U.S. Department of Agriculture, Economic Research Service, 2014.
2 *Deposition technologies for films and coatings: developments and applications*, ed. R. F. Bunshah, Noyes Publications, Park Ridge, NJ, 1982.
3 K. Willard, *Agriculture center aims to use soft drink waste*, Western Farm Press, 2011.
4 M. E. Boot-Handford, J. C. Abanades, E. J. Anthony, M. J. Blunt, S. Brandani, N. Mac Dowell, J. R. Fernandez, M.-C. Ferrari, R. Gross, J. P. Hallett, R. S. Haszeldine, P. Heptonstall, A. Lyngfelt, Z. Makuch, E. Mangano, R. T. J. Porter, M. Pourkashanian, G. T. Rochelle, N. Shah, J. G. Yao and P. S. Fennell, *Energy Environ. Sci.*, 2014, **7**, 130–189.
5 Y. Dong, L. Wan, J. Cai, Q. Fang, Y. Chi and G. Chen, *Sci. Rep.*, 2015, 5.
6 Q. Liang, W. Ma, Y. Shi, Z. Li and X. Yang, *Carbon*, 2013, **60**, 421–428.
7 W. Du, X. Xu, H. Hao, R. Liu, D. Zhang, F. Gao and Q. Lu, *Sci. China: Chem.*, 2015, **58**, 863–870.
8 Y. Wang and A. Hu, *J. Mater. Chem. C*, 2014, **2**, 6921–6939.
9 Y.-P. Sun, B. Zhou, Y. Lin, W. Wang, K. A. S. Fernando, P. Pathak, M. J. Meziani, B. A. Harruff, X. Wang, H. Wang, P. G. Luo, H. Yang, M. E. Kose, B. Chen, L. M. Veca and S.-Y. Xie, *J. Am. Chem. Soc.*, 2006, **128**, 7756–7757.
10 S. Sahu, B. Behera, T. K. Maiti and S. Mohapatra, *Chem. Commun.*, 2012, **48**, 8835–8837.
11 P. K. Sarswat and M. L. Free, *J. Cryst. Growth*, 2013, **372**, 87–94.
12 Y. Wang, L. Dong, R. Xiong and A. Hu, *J. Mater. Chem. C*, 2013, **1**, 7731–7735.
13 K. A. S. Fernando, S. Sahu, Y. Liu, W. K. Lewis, E. A. Guliants, A. Jafariyan, P. Wang, C. E. Bunker and Y.-P. Sun, *ACS Appl. Mater. Interfaces*, 2015, **7**, 8363–8376.
14 A. Bhattacharya, S. Chatterjee, R. Prajapati and T. K. Mukherjee, *Phys. Chem. Chem. Phys.*, 2015, **17**, 12833–12840.
15 S. Hu, R. Tian, Y. Dong, J. Yang, J. Liu and Q. Chang, *Nanoscale*, 2013, **5**, 11665–11671.
16 Z. Gao, G. Shen, X. Zhao, N. Dong, P. Jia, J. Wu, D. Cui, Y. Zhang and Y. Wang, *Nanoscale Res. Lett.*, 2013, **8**, 276.
17 A. L. Merrill and B. K. Watt, *Energy value of foods: basis and derivation*, U.S. Government Printing Office, Washington, DC, 1973, vol. 24.
18 L. Silveira Jr., L. M. Moreira, V. G. B. Conceição, H. L. Casalechi, I. S. Muñoz, F. F. Da Silva, M. A. S. R. Silva, R. A. De Souza and M. T. T. Pacheco, *Spectroscopy*, 2009, 23.
19 B. R. Singh, M. A. Wechter, Y. Hu and C. Lafontaine, *Biochem. Educ.*, 1998, **26**, 243–247.
20 L. C. Bichara, H. E. Lanús, E. G. Ferrer, M. B. Gramajo and S. Brandán, *Adv. Phys. Chem.*, 2011, **2011**, 347072, DOI: 10.1155/2011/347072.
21 M. M. Paradkar and J. Irudayaraj, *J. Food Sci.*, 2002, **67**, 2507–2511.
22 H. K. Khurana, I. K. Cho, J. Y. Shim, Q. X. Li and S. Jun, *J. Agric. Food Chem.*, 2008, **56**, 778–783.
23 M. Soylak, Y. E. Unsal, E. Yilmaz and M. Tuzen, *Food Chem. Toxicol.*, 2011, **49**, 1796–1799.
24 L. Lin and S. Zhang, *Chem. Commun.*, 2012, **48**, 10177–10179.
25 Y. Pugen, Q. Haiou, L. Cuili and T. Zhiyong, *Int. J. Spectrosc.*, 2011, **2011**, 281931.

26 G.-p. Cao, T. Chen and Y.-f. Zhuang, *J. Fluoresc.*, 2013, **23**, 641–647.
27 G. D. Saraiva, C. E. S. Nogueira, P. T. C. Freire, F. F. de Sousa, J. H. da Silva, A. M. R. Teixeira and J. Mendes Filho, *Spectrochim. Acta, Part A*, 2015, **137**, 1409–1416.
28 K. Ilaslan, I. H. Boyaci and A. Topcu, *Food Control*, 2015, **48**, 56–61.
29 W. W. Rudolph, *Dalton Trans.*, 2010, **39**, 9642–9653.
30 K. Hola, A. B. Bourlinos, O. Kozak, K. Berka, K. M. Siskova, M. Havrdova, J. Tucek, K. Safarova, M. Otyepka, E. P. Giannelis and R. Zboril, *Carbon*, 2014, **70**, 279–286.
31 L. Cao, M. J. Meziani, S. Sahu and Y.-P. Sun, *Acc. Chem. Res.*, 2013, **46**, 171–180.
32 L. Wang, S.-J. Zhu, H.-Y. Wang, S.-N. Qu, Y.-L. Zhang, J.-H. Zhang, Q.-D. Chen, H.-L. Xu, W. Han, B. Yang and H.-B. Sun, *ACS Nano*, 2014, **8**, 2541–2547.
33 H. Li, X. He, Z. Kang, H. Huang, Y. Liu, J. Liu, S. Lian, C. H. A. Tsang, X. Yang and S.-T. Lee, *Angew. Chem., Int. Ed.*, 2010, **49**, 4430–4434.
34 L. Brus, *J. Phys. Chem.*, 1986, **90**, 2555–2560.
35 D. Di, K. P. Musselman, G. Li, A. Sadhanala, Y. Ievskaya, Q. Song, Z.-K. Tan, M. L. Lai, J. L. MacManus-Driscoll, N. C. Greenham and R. H. Friend, *J. Phys. Chem. Lett.*, 2015, **6**, 446–450.
36 M. Roy and P. A. Maksym, *Phys. Rev. B: Condens. Matter Mater. Phys.*, 2012, **85**, 205432.
37 P. Jarillo-Herrero, S. Sapmaz, C. Dekker, L. P. Kouwenhoven and H. S. J. van der Zant, *Nature*, 2004, **429**, 389–392.
38 S. Sreekala, X. H. Peng, P. M. Ajayan and S. K. Nayak, *Phys. Rev. B: Condens. Matter Mater. Phys.*, 2008, **77**, 155434.
39 M. R. C. Hunt and R. E. Palmer, *The development of metallic behaviour in clusters on surfaces*, 1998.
40 R. Kubo, *J. Phys. Soc. Jpn.*, 1962, **17**, 975–986.
41 C. Liang and H. F. Schaefer, *Chem. Phys. Lett.*, 1990, **169**, 150–160.
42 S. Saito, S. Okada, S.-i. Sawada and N. Hamada, *Phys. Rev. Lett.*, 1995, **75**, 685–688.
43 X. Li, S. Zhang, S. A. Kulinich, Y. Liu and H. Zeng, *Sci. Rep.*, 2014, 4.
44 S. Zhu, Y. Song, X. Zhao, J. Shao, J. Zhang and B. Yang, *Nano Res.*, 2015, **8**, 355–381.
45 S. Zhu, L. Wang, B. Li, Y. Song, X. Zhao, G. Zhang, S. Zhang, S. Lu, J. Zhang, H. Wang, H. Sun and B. Yang, *Carbon*, 2014, **77**, 462–472.
46 L. Bao, C. Liu, Z.-L. Zhang and D.-W. Pang, *Adv. Mater.*, 2015, **27**, 1663–1667.
47 C. Netzel, V. Hoffmann, T. Wernicke, A. Knauer, M. Weyers, M. Kneissl and N. Szabo, *J. Appl. Phys.*, 2010, **107**, 033510.
48 X. Yu, R. Liu, G. Zhang and H. Cao, *Nanotechnology*, 2013, **24**, 335401.
49 X. Zhai, P. Zhang, C. Liu, T. Bai, W. Li, L. Dai and W. Liu, *Chem. Commun.*, 2012, **48**, 7955–7957.
50 A. Flores-Morales, M. Jiménez-Estrada and R. Mora-Escobedo, *Carbohydr. Polym.*, 2012, **87**, 61–68.
51 Z. Li, H. Yu, T. Bian, Y. Zhao, C. Zhou, L. Shang, Y. Liu, L.-Z. Wu, C.-H. Tung and T. Zhang, *J. Mater. Chem. C*, 2015, **3**, 1922–1928.
52 R. Zhang and W. Chen, *Biosens. Bioelectron.*, 2014, **55**, 83–90.
53 Q. Li, S. Zhang, L. Dai and L.-S. Li, *J. Am. Chem. Soc.*, 2012, **134**, 18932–18935.
54 Y. Wang, S. Kalytchuk, L. Wang, O. Zhovtiuk, K. Cepe, R. Zboril and A. L. Rogach, *Chem. Commun.*, 2015, **51**, 2950–2953.
55 C.-L. Li, C.-C. Huang, A. P. Periasamy, P. Roy, W.-C. Wu, C.-L. Hsu and H.-T. Chang, *RSC Adv.*, 2015, **5**, 2285–2291.
56 W. Chung, H. Jung, C. H. Lee and S. H. Kim, *J. Mater. Chem. C*, 2014, **2**, 4227–4232.
57 X. Zhang, Y. Zhang, Y. Wang, S. Kalytchuk, S. V. Kershaw, Y. Wang, P. Wang, T. Zhang, Y. Zhao, H. Zhang, T. Cui, Y. Wang, J. Zhao, W. W. Yu and A. L. Rogach, *ACS Nano*, 2013, **7**, 11234–11241.
58 X. Li, Y. Liu, X. Song, H. Wang, H. Gu and H. Zeng, *Angew. Chem., Int. Ed.*, 2015, **54**, 1759–1764.
59 J. Xu, S. Sahu, L. Cao, C. E. Bunker, G. Peng, Y. Liu, K. A. S. Fernando, P. Wang, E. A. Guliants, M. J. Meziani, H. Qian and Y.-P. Sun, *Langmuir*, 2012, **28**, 16141–16147.
60 Y. Wang, S. Kalytchuk, Y. Zhang, H. Shi, S. V. Kershaw and A. L. Rogach, *J. Phys. Chem. Lett.*, 2014, **5**, 1412–1420.

